ACS SENSORS

Article

Cite This: ACS Sens. 2019, 4, 2825−2831

pubs.acs.org/acssensors

Electrochemiluminescence Double Quenching System Based on Novel Emitter $GdPO_4$:Eu with Low-Excited Positive Potential for Ultrasensitive Procalcitonin Detection

Jingwei Xue,[†] Lei Yang,[†] Yue Jia,[†] Huan Wang,[†] Nuo Zhang,[†] Xiang Ren,[†] Hongmin Ma,*[,†] Qin Wei,[†] and Huangxian Ju[†,‡]

[†]Key Laboratory of Interfacial Reaction & Sensing Analysis in Universities of Shandong, School of Chemistry and Chemical Engineering, University of Jinan, Jinan 250022, P. R. China

[‡]Key Laboratory of Analytical Chemistry for Life Science, School of Chemistry and Chemical Engineering, Nanjing University, Nanjing 210023, P. R. China

Supporting Information

ABSTRACT: Nowadays, the electrochemiluminescence (ECL) immunosensor with the unique superiority of tunable luminescence and ultrahigh sensitivity has become one of the most promising immunoassay techniques, especially for low-abundance biomarkers analysis. However, the use of signal probes with high excited potential and applied emitters which owned good intensity but biotoxicity limited its application. Herein, an ECL resonance energy transfer strategy was developed based on protein bioactivity protection utilizing europium-doped phosphoric acid gadolinium ($GdPO_4$:Eu) as novel low-potential luminophor (donor) and Pd@Cu_2O as the quenching probe (acceptor). Specifically, $GdPO_4$:Eu was first prepared by using the hydrothermal synthesis method to apply in ECL, and when it coexisted with $K_2S_2O_8$, cathode, a strong ECL signal would be generated at a low potential of −1.15 V (vs Ag/AgCl), where the immunocompetence of antigens and antibodies can be maintained well. Electrical pair Eu^{3+}/Eu^{2+}, as the coreactant promoter, produced by potential excitation could produce more $SO_4^{\bullet-}$ to accelerate the oxidation process of $GdPO_4$:Eu. Meanwhile, Cu_2O coated onto Pd (Pd@Cu_2O), as a dual-quencher, enhanced the quenching effect of Pd alone and controlled the ECL intensity of the "signal on" state within a reasonable range. As a result, the proposed biosensor for detection of trace procalcitonin, a biomarker of systemic inflammatory response syndrome, exhibited a far low detection limit, 0.402 fg/mL (S/N = 3). Importantly, this work not only utilized a promising ECL emitter for biosensing platform construction but also had momentous potential in biomarker detection of disease diagnosis and clinical analysis.

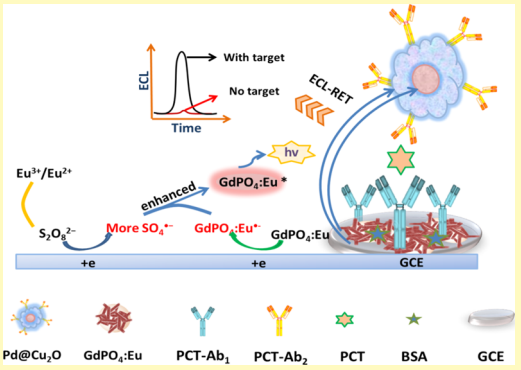

KEYWORDS: *phosphoric acid gadolinium, low-potential, electrochemiluminescence, dual-quenching, cuprous oxide*

Electrochemiluminescence (ECL),[1] which possesses a wide dynamic range, high sensitivity, facility, and good stability, has been widely applied in environmental analysis and biochemical and clinical examination.[2] Although traditional luminophors, such as g-C_3N_4 and $Ru(bpy)_3^{2+}$ or Cd-based compound, have the advantages of good luminous properties,[3] the difficulty of immobilization on electrodes because of their satisfied water solubility or biological toxicity caused a serious negative effect, which reduced their application on ECL.[4] Recently, many researchers have obtained satisfactory results by replacing toxic signal probes with optical materials that possess good biocompatibility and excellent electrode adsorption.[5] However, the irreversible oxidative damage to the oligonucleotide sequences is often overlooked when the excitation potential is excessive.[6] This means that the control of scanning potential should be tightened when ECL technology is applied in immunoassay.[7] In our previous work,[8] this aspect has been mentioned and some corresponding proof experiment has been done in the positive potential range.[9] Therefore, the discovery and exploration of novel low-potential luminophor with good biocompatibility in the application of immunoassay has become the core of this work.

Hollow nanomaterials have unique properties like controllable size and morphology and have become a hot issue in the fields of biochemistry research.[10] Their functional materials by modifying the sphere surface are generally widely used in biosensors and drug or carrier delivery. Nowadays, gadolinium-based nanomaterials are considered to be a promising optical multifunctional nanoplatform.[11] On the one hand, because of the huge number of unpaired electrons in Gd^{3+}, gadolinium-based nanomaterials have great application potential in energy excitation and transmission.[11] On the other hand, some of

Received: August 12, 2019
Accepted: October 7, 2019
Published: October 7, 2019

DOI: 10.1021/acssensors.9b01552
ACS Sens. 2019, 4, 2825−2831

Scheme 1. Schematic Representation of the Fabrication of the Immunosensor

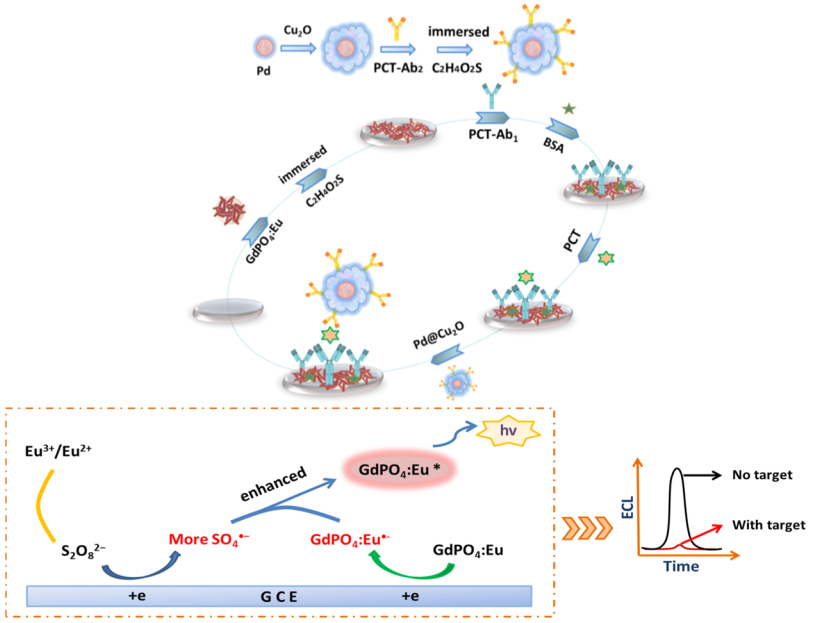

lanthanide activator ion-doped gadolinium orthophosphate ($GdPO_4$) due to the advantages of low toxicity have been diffusely investigated in the field of fluorescence,[12] but there have been no reports on the ECL behavior of $GdPO_4$ as far as we know.

All the time, Eu-doped $GdPO_4$ gets a high profile because of satisfactory energy transfer between Gd^{3+} and Eu ions in $GdPO_4$:Eu nanomaterials in the field of fluorescence.[13] Here, $GdPO_4$ and Eu-doped $GdPO_4$ ($GdPO_4$:Eu) with good biocompatibility and adsorption were synthesized by the template method and their ECL intensity was compared by using the experiment,[14] which proved that the doping of Eu is conducive to enhance the ECL efficiency.[15] Zeng's group utilized hemin as the coreaction promoter designed in an ECL aptasensor to catalyze $S_2O_8^{2-}$ for accelerating the oxidation process of PTCA.[16] Therefore, one hypothesis is that it is not difficult for Eu^{3+}/Eu^{2+} as the coreactant accelerator to achieve recycling via electrochemical redox reaction.

Palladium nanoparticles (Pd NPs) and cuprous oxide (Cu_2O) have been widely used in photocatalysis,[17] photoelectric, and other electrochemical fields[18] because of their good and wide ultraviolet absorption (UV−vis) range, which could be applied in quenching of resonance energy transfer (RET).[19] The optical properties of Au−Cu_2O core−shell nanocrystals can be affected by its surface states. Based on this current research, the well-dispersed core−shell structure of Pd@Cu_2O, as a dual-quencher, was synthesized by coating Cu_2O onto the Pd core like popcorn.[20] More fortunately, the UV−vis spectra of Pd@Cu_2O were found to overlap effectively with ECL emission of $GdPO_4$:Eu, which increased the area more than that of Pd alone. Herein, the obtained effect not only obtained quenching efficiency better but also increased the biosensor sensitivity.[21]

From what has been discussed above, it is worth highlighting that based on the protection of the protein activity to antigens and antibodies, biocompatible $GdPO_4$:Eu was put forward in the field of ECL with a strong self-enhanced ECL signal at a low-potential of −1.15 V (vs Ag/AgCl) for the first time. Potassium peroxodisulfate ($K_2S_2O_8$) was chosen as the coreactant, and the Eu/Eu^{2+} redox-pair acted as a novel coreactive promoter so that the $GdPO_4$:Eu/$K_2S_2O_4$ system could obtain strongly stimulated intensity. Core−shell Pd@Cu_2O was selected as a dual-quencher which could maximize the effective quenching to meet the "signal on" state into a suitable intensity.[22] Significantly, the bioactivity-protected ECL "signal on−off" system was not only proposed with a super low detection limit toward procalcitonin (PCT) of 0.402 fg/mL but also opened a new way for highly sensitive and selective detection of other biomarkers in disease diagnosis and clinical analysis.[23]

MATERIAL AND METHODS

Preparation of $GdPO_4$:Eu Hollow Spheres. The monodisperse APF resin template and APF@$Gd(OH)CO_3$ precursor were synthesized and modified on the basis of previous research.[24] The detailed experimental procedures are shown in the Supporting Information. First, the precursor APF@$Gd(OH)CO_3$ was dispersed into 25 mL of deionized water under the hyperacoustic condition. Then, the solution of 0.1150 g of $NH_4H_2PO_4$ dissolved in 10 mL of H_2O was added dropwise to the above solution. After 10 min of stirring, 0.1333 g of CTAB was further added, and then the mixed solution was transferred into a 50 mL autoclave and heated for 12 h at 180 °C. The product (APF@$GdPO_4$) was separated and washed. Finally, APF@$GdPO_4$ was annealed at 500 °C for 2 h to obtain the hollow spheres $GdPO_4$. The $GdPO_4$:Eu spheres were fabricated by a similar procedure except for adding $Eu(NO_3)_3$ (molar ratio, 5%) instead of the same dose $Gd(NO_3)_3$ at the initial stage.

Preparation of Pd NPs. The method used was based on previous experience and few improvements were made.[20] First, 0.048 g of CTAC, 9.125 mL of deionized water, and 0.7 mL of 10 mM H_2PdCl_4 solution were introduced to a small beaker. The beaker was kept in a 35 °C water bath. Next, 500 μL of 1 mM KBr solution and 50 μL of 1 mM KI solution were added and well-mixed. Then, 1.2 mL of 0.05 M ascorbic acid was injected after 10 min and further kept for 30 min in water bath. The final product was obtained by centrifugation twice at 8000 rpm of 10 min and dispersed in 500 μL of deionized water.

Synthesis of Pd−Cu_2O Core−Shell Nanocrystals. Briefly, 0.087 g of SDS was dissolved in deionized water, and 0.07 mL of 0.1 M $CuCl_2$ solution and 0.04 mL of Pd solution was introduced. Then, 0.25 mL of 1.0 M NaOH and 0.15 mL of 0.2 M $NH_2OH{\cdot}HCl$ solutions were injected with a 10 s interval between their

DOI: 10.1021/acssensors.9b01552
ACS Sens. 2019, 4, 2825−2831

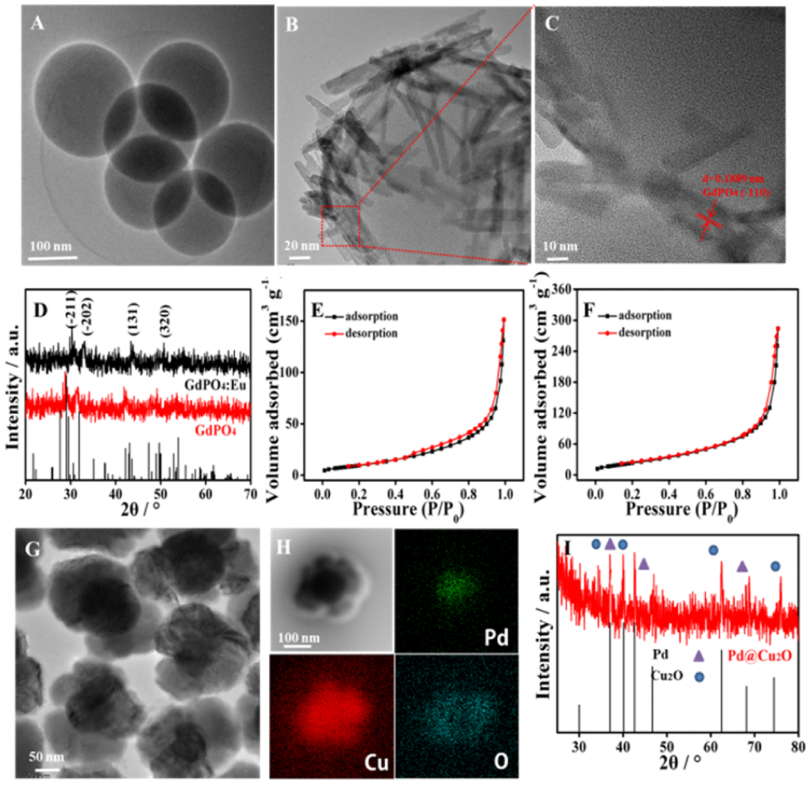

Figure 1. SEM image of APF (A), TEM image (B), and HRTEM (C) of $GdPO_4$:Eu, XRD spectra of $GdPO_4$:Eu and $GdPO_4$ (D), N_2 adsorption isotherms of the precursor of APF@$Gd(OH)CO_3$ (E), $GdPO_4$:Eu (F), TEM image (G), and the corresponding mapping (H) of Pd@$Cu_2O$and XRD spectra of Pd@Cu_2O (I).

introduction. After 2 h, the nanocrystal was centrifuged at 5000 rpm for 3 min followed by washing with deionized water and ethanol in a 1:1 volume ratio three times.

Synthesis of Pd@Cu_2O−Ab_2 Biological Complex. The obtained Pd@Cu_2O above was immersed into 10 mL PBS containing the mixture of 0.1 M NaCl and 3 mM $C_2H_4O_2S$ at 4 °C for 5 h to attract carboxyl groups and then added in 0.01 M EDC/NHS in 1:1 volume ratio activation. After each step, wash by using 10 mM PBS (pH = 7.4).[25]

Fabrication of the Immunosensor. First, a glassy carbon electrode (GCE) with a diameter of 4.0 mm was pretreated.[26] Then, it was modified with 6 μL of $GdPO_4$:Eu. After drying, GCE/$GdPO_4$:Eu was immersed into PBS which contained 0.1 M NaCl and 3 mM $C_2H_4O_2S$ for 5 h at 4 °C and then activated by 0.01 M EDC/NHS in 1:1 volume ratio activation. After that, the electrode was dipped into Ab_1 (5 μg/mL) at 4 °C for 12 h layer with active carboxyl groups. Then, 3 μL of BSA (0.1%) was also dropped onto the surface. Next, 6 μL of PCT was incubated at 37 °C overnight, followed by modifying 6 μL of Pd@Cu_2O−Ab_2 and dried. The assembly process of this biosensor is depicted in Scheme 1.

ECL Measurements. The electrochemical measurement was demonstrated by utilizing cyclic voltammetry (CV) with the potential range of −1.15−0 V (vs Ag/AgCl) at 0.12 V/s scanning rate with a three-electrode system (Supporting Information).[27] The detection was worked in 10 mL of $K_2S_4O_8$ (1 mM, pH 7.6) with the voltage of 750 V for the photomultiplier tube.[28]

RESULTS AND DISCUSSION

Material Characterization. The monodisperse APF spheres shown by the scanning electron microscope (SEM) possessed an average diameter of 200 nm (Figure S2A), which was further proved by transmission electron microscopy[19] as shown in Figure 1A. When $GdPO_4$:Eu is grown onto APF, TEM images (Figures S2B and 1B) could prove its rod-like structure with a relatively homogeneous state. X-ray diffraction (XRD) (Figure 1D) was applied to characterize $GdPO_4$ and $GdPO_4$:Eu crystallization. Specific peaks were found at 30.883°, 35.093°, 45.740°, and 50.033°, which corresponded to the (−211), (−202), (131), and (320) planes of $GdPO_4$, respectively (JCPDS Card no. 32-0386). When Eu was doped onto $GdPO_4$, there is a much slight shift in the peak position but it did not affect the peak shape, which means that there was no effect on the lattice of $GdPO_4$ and Eu being successfully doped. Besides, high-resolution transmission electron microscopy (HRTEM) was used to demonstrate the existence of representative lattice (Figure 1C). TEM mapping was also utilized to observe the distribution of elements in Figure S2C−H. Furthermore, N_2 adsorption isotherms of the precursor of $GdPO_4$:Eu (APF@$Gd(OH)CO_3$) and $GdPO_4$:Eu were also tested by the method of Barrett−Joyner−Halenda. Comparing $GdPO_4$:Eu (Figure 1F) to APF@$Gd(OH)CO_3$ (Figure 1E), the specific surface area of $GdPO_4$:Eu (19.03 m^2/g) was nearly five times larger than APF@$Gd(OH)CO_3$ (90.21 m^2/g), which indicated the advantage of a huge specific surface area.

Moreover, Pd cores and Pd@Cu_2O core−shell nanocrystals were represented by similar means. Pd cores were shown by SEM images with the average diameters about 180 nm (Figure S2I) and the energy dispersive spectrometer (EDS) was used to further confirm its successful preparation (Figure S2K). Cu_2O was coated onto the Pd cores and the Pd@Cu_2O core−shell nanocrystals were prepared. SEM was applied to view morphology and the average diameter of Pd@Cu_2O was shown to be about 220 nm (Figure S2J). TEM was employed to further confirm the morphology. The prominent core−shell structure was clearly shown in Figure 1G. EDS (Figure S2L) and TEM mapping (Figure 1H) were utilized to prove the

DOI: 10.1021/acssensors.9b01552
ACS Sens. 2019, 4, 2825−2831

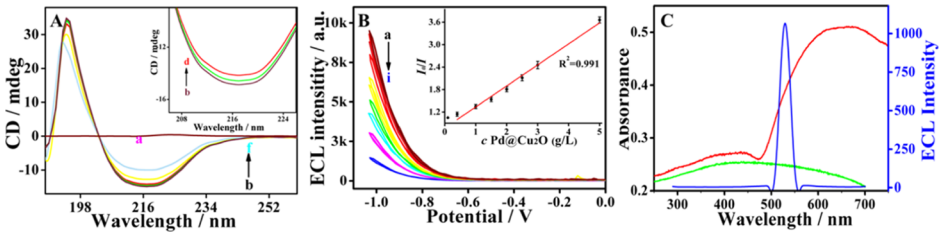

Figure 2. CD spectra of PCT (0.5 mg/mL) stimulated by different potential (A), the ECL intensity of modifying different concentration of Pd@Cu_2O (B) and the plot of I_0/I vs concentrations of Pd@Cu_2O (inset of B), overlaps between the $GdPO_4$:Eu ECL emission (curve blue) and Pd cores UV−vis spectra (curve green) or Pd@Cu_2O (curve red) (C).

element composition intuitively. XRD (Figure 1I) was employed to characterize the crystallization of Pd@Cu_2O. Peaks of different planes of Pd were displayed at 40.118°, 46.658°, and 68.119°, which corresponded to the (111), (200) and (220) planes, respectively (JCPDS Card no. 46-1043). Meanwhile, peaks of Cu_2O were found at 29.981°, 37.009°, 42.611°, 62.444°, and 74.402°, which, respectively, corresponded to planes of (110), (111), (200), (220), and (311) (JCPDS Card no. 34-1354). All the results indicated that the preparation of $GdPO_4$:Eu and Pd@Cu_2O in this work was successful.

PCT Bioactivity Analysis and Mechanism Investigation of the "Signal On−Off" System. The activity of the immune contents observing the change of conformation can be mirrored by utilizing CD spectra with 0.5 mg/mL PCT stimulated by different potential (Figure 2A). The PCT samples were using CV scanning by adjusting the potential −1 to 0 (b), −1.2 to 0 (c), −1.5 to 0 (d), −1.8 to 0 (e), −2 to 0 V (f) at 4 °C with a three-electrode system, where the other experimental conditions remained unchanged. Particular analysis details are in the Supporting Information. From the experimental results, it is astonishing for us to observe that the MRE of PCT decreased half nearly when the original sample was −2 to 0 V compared to that with the excitation potential −1 to 0 V. The results proved that the low potential would not cause significant changes in protein activity, which at the same time proved the huge degree of potential could lead protein into irreversible damage, especially more less than −1.2 V. On account of this, more attention to the bioactivity protection of protein should be paid instead of widely exploring materials alone in ECL immunoassay. The favorable low potential of $GdPO_4$:Eu and the ability to reach excellent stability become its great advantages.

When the coreactant $K_2S_2O_8$ acted on $GdPO_4$:Eu, the possible enhancement mechanism was as follows: $GdPO_4$:$Eu^{\bullet-}$ was first generated at the electrode surface when the system was beginning to work, and then, it reacted with $SO_4^{\bullet-}$ which decomposed from $S_2O_8^{2-}$ because the potential motivates to form the excited-state $GdPO_4$:Eu* which backed to the ground state with emitting light. Oxidation−reduction pair Eu^{3+}/Eu^{2+} acted as the co-reaction accelerator which could react with $S_2O_8^{2-}$ to produce more $SO_4^{\bullet-}$.[29] Under voltage excitation, the oxidation−reduction pair Eu^{3+}/Eu^{2+} would be produced when electron is captured by Eu^{3+}. Furthermore, the ECL intensity of $GdPO_4$ and $GdPO_4$:Eu was first applied to compare (Figure S3). It could be observed that when Eu doped, the intensity became around 3 times higher than that without Eu. It also demonstrated that Eu^{3+}/Eu^{2+} acted as an efficient coreaction accelerator to speed up the reduction of $S_2O_8^{2-}$ to produce more $SO_4^{\bullet-}$ and thus achieving a huge emission of $GdPO_4$:Eu*. The possible enhanced principles were described by equations as follows

$$GdPO_4{:}Eu + e^- \rightarrow GdPO_4{:}Euo^{\bullet-}$$

$$S_2O_8^{2-} + e^- \rightarrow SO_4^{\bullet-}$$

$$Eu^{3+} + e^- \rightarrow Eu^{2+}$$

$$Eu^{2+} + S_2O_8^{2-} \rightarrow Eu^{3+} + SO_4^{2-} + (more)SO_4^{\bullet-}$$

$$SO_4^{\bullet-} + GdPO_4{:}Eu^{\bullet-} \rightarrow GdPO_4{:}Eu^* + SO_4^{2-}$$

$$GdPO_4{:}Eu^* \rightarrow GdPO_4{:}Eu + h\nu$$

When it comes to the possible dual-quenching principle of Pd@Cu_2O (acceptor) toward the $GdPO_4$:Eu (donor) system, the layer of GCE/$GdPO_4$:Eu−Ab_1/BSA/PCT electrode acted as the initial ECL probe, and the ECL quenching effect was investigated by adding a series of concentrations of Pd@Cu_2O onto the initial electrode in 10 mL of $K_2S_2O_8$ (pH 7.6). The Pd@Cu_2O concentration (g/L) of 0.05 (a), 0.1 (b), 0.5 (c), 1.0 (d), 1.5 (e), 2.0 (f), 2.5 (g), 3.0 (h), 5 (i) were detected using the proposed biosensor. As concentration of Pd@Cu_2O increased, the ECL intensity decreased, as shown in Figure 2B. The inset of Figure 2B shows the plot of I_0/I versus concentrations of Pd@Cu_2O with a range of 0.05−5 g/L (R^2 = 0.99), indicating that the mechanism of quenching described by the Stern−Volmer equation could be established.[30] The quenching constant (K_{sv}) was measured at 5.611×10^5 g^{-1}, where I represents the ECL intensity with Pd@Cu_2O and I_0 without. Furthermore, it was mainly given the credit to ECL−RET between their two. Satisfactory overlaps were studied between $GdPO_4$:Eu ECL emission (curve blue) and Pd cores UV−vis spectra (curve green) or Pd@Cu_2O (curve red) (Figure 2C). When Cu_2O was coated onto the Pd core, it gained more overlaps than Pd, while the dual-quenching effect by Pd@Cu_2O toward $GdPO_4$:Eu was confirmed.

Characterization of the Immunosensor. At the beginning, GCE/$GdPO_4$:Eu was tested by CV (Figure 3A) with a different scanning speed range of 0.02−0.38 V/s in the mixed solution (2.5 mM $Fe(CN)_6^{3-/4-}$ and 0.1 M KCl) to calculate the electrochemical active electrode area. The standard curve, $i \times 10^{-6}(A) = -262.68(v^{1/2}/s^{1/2}) - 0.34421$, was drawn with i_{pc} as the ordinate and $v^{1/2}$ as the abscissa (Figure 3B). This plot revealed with clear linear relation, which further indicated there was only controlled by diffusion on the electrode surface.

According to the Randles−Sovcik equation

$$i_{ps} = 2.69 \times 10^5 n^{3/2} D^{1/2} v^{1/2} AC \quad (1)$$

DOI: 10.1021/acssensors.9b01552
ACS Sens. 2019, 4, 2825−2831

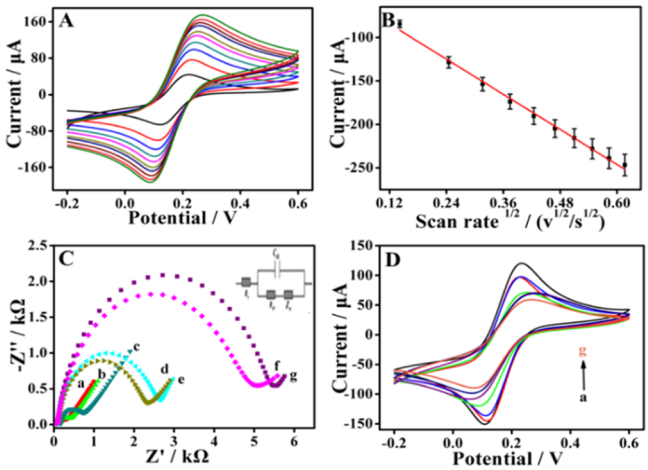

Figure 3. CV curves (A) of $GdPO_4$:Eu with scanning speeds of 0.02−0.38 V/s and its standard curve (B), EIS responses (C), and CV (D) of the biosensor with following modified states: (a) bare GCE, (b) GCE/$GdPO_4$:Eu, (c) GCE/$GdPO_4$:Eu−$C_2H_4O_2S$, (d) GCE/$GdPO_4$:Eu−$C_2H_4O_2S$/Ab_1, (e) GCE/$GdPO_4$:Eu−$C_2H_4O_2S$/Ab_1/BSA, GCE/$GdPO_4$:Eu−$C_2H_4O_2S$/Ab_1/BSA/PCT, and (g) GCE/$GdPO_4$:Eu−$C_2H_4O_2S$/Ab_1/BSA/PCT/Pd@Cu_2O−Ab_2.

$$A = \frac{k}{2.69 \times 10^5 n^{3/2} D_0^{1/2} C_0} \quad (2)$$

Among them, i_{ps} is the peak m reduction current of $K_3Fe(CN)_6$, n is the number of electrons transferred during the oxidation−reduction reaction of $K_3Fe(CN)_6$ (n is the number of electrons transferred in the REDOX reaction, n = 1), A is electrode electrochemical active area (cm^2), D is the diffusion coefficient of $K_3Fe(CN)_6$ ($D_0 = 1 \times 10^{-5}$ cm^2/s), C is the concentration of $K_3Fe(CN)_6$ ($C_0 = 2.5 \times 10^{-3}$ mol/L), v is the scanning speed (k = 0.241). First, the peak current of GCE/$GdPO_4$:Eu was measured and the peak current value of 1.233×10^{-4} A was obtained, and the obtained effective electrochemical active area calculated by eq 1 is 0.3240 cm^2, which is 2.58 times of the actual area (Φ = 4 mm, 0.1256 cm^2). It is worth mentioning that such a huge active area would increase the catalytic site and accelerate the redox process on the electrode surface.[31]

Besides, different modified states of electrodes were studied by electrochemical impedance spectroscopy (EIS) for fabrication of the biosensor in 2.5 mM $[Fe(CN)_6]^{3-/4-}$ containing 0.1 M KCl. The bare GCE (curve a) was only a small impedance value because of diffusion (Figure 3C). After being dropped onto $GdPO_4$:Eu (curve b), soaked into thioglycolic acid (curve c), incubated Ab_1 (curve d) and modified with BSA (curve e), PCT (curve f), and Pd@Cu_2O−Ab_2 (curve g), the semicircle of impedance gradually increased, especially after the attachment of antigens and antibodies, the impedance increased significantly. This was due to the fact that the protein blocked electron transfer and reduced the conductivity of electrode's surface, suggesting that the sensor was built successfully. In addition, the equivalent circuit element of simulation parameters was simulated for the circuit to reveal the impedance (Table S1). CV scanning was an important method to characterize the assembly process of the biosensor, which could clarify the interface properties of the electrodes and further improve the reliability of EIS results. Thus, the corresponding CV scanning of EIS electrode states was also done (Figure 3D). In brief, the proposed ECL biosensor was constructed successfully based on all the results.

PCT Analysis. The proposed ECL−RET strategy between $GdPO_4$:Eu and Pd@Cu_2O was utilized for the measure of PCT with different concentrations from 10 fg/mL to 500 ng/mL. Figure 4A,B exhibited raw data and the standard curve,

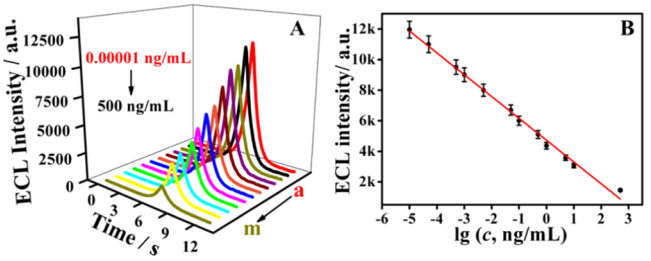

Figure 4. Detection of PCT with different concentrations from 10 fg/mL to 500 ng/mL (A) and exhibited standard curve (B) detected with 10 mL of $K_2S_2O_8$ (1 M, pH 7.6).

respectively. The standard curve, $I_{ECL} = 4730.26 - 1427.43 \times \lg c$ (R^2 = 0.995), made log c as the X-axis and ECL intensity I_{ECL} as the Y-axis with a detection limit of 0.402 fg/mL (S/N = 3), which is far lower than that of other detection methods (Table S2). Therefore, results obtained of this system could provide a vital direction to PCT detection and other biomarkers' measurement.

Analysis of the Real Sample. The real serum sample analysis was included to adequately reflect the potential of the biosensor. Nowadays, systemic inflammatory response syndrome (SIRS) is no effective treatment toward the disease.[32] PCT, a typical biomarker of SIRS, played an important role in the early defense of SIRS.[33] The value of PCT detected by the proposed biosensor in the obtained human serum was 0.120, 0.031, and 3.58 ng/mL. The recovery rate investigated biosensor application was achieved by the method of standard recovery (Table 1), which display a recovery range of 98.2−102% (n = 5) and RSD under 2.66%. If it has prominent difference in accuracy, it should be performed by the F-test to judge. The F value (s was on behalf of the standard deviation)

Table 1. Recoveries of PCT in Serum Samples of Different Concentrations

sample (ng/mL)	addition content (ng/mL)	detection content (ng/mL)	RSD (%, n = 5)	recovery (%)
3.581	1.00	4.56, 4.52, 4.58, 4.63, 4.62	1.01	98.2
	3.00	6.59, 6.41, 6.63, 6.57, 6.65	1.44	99.7
	5.00	8.48, 8.62, 8.55, 8.63, 8.54	0.61	99.6
0.120	0.10	0.24, 0.25, 0.23, 0.27, 0.21	1.62	102
	0.30	0.47, 0.40, 0.44, 0.49, 0.45	0.76	101
	0.50	0.64, 0.68, 0.65, 0.60, 0.63	0.55	99.9
0.031	0.01	0.047, 0.040, 0.044, 0.043, 0.041	2.66	99.6
	0.03	0.065, 0.062, 0.069, 0.067, 0.066	0.92	99.8
	0.05	0.085, 0.089, 0.087, 0.086, 0.088	1.29	99.7

DOI: 10.1021/acssensors.9b01552
ACS Sens. 2019, 4, 2825−2831

was calculated at 1.25 (eq 3), which was under the theoretical one (F = 6.39 with 95% confidence limits). Both of two methods possessed highly equivalent precisions. Meanwhile, this biosensor was respectively with human serum assessed by the ELISA kit for five times. The average value designed by standard recovery was of no significant difference from that of ELISA. The T-test (Table S3) was also applied to evaluate this dual-quenching system (Equation 4) and the t value was calculated by taking the ratio of the absolute value of the mean of the two methods ($|\overline{X} - \mu|$) to the standard deviation (s). Herein, the value of t was at 1.79, under 2.57 (P = 0.95, α = 0.05, f = 4), which demonstrated that the system error could be neglected. By the F-test and t-test, the precision and accuracy can be guaranteed.[34]

$$F = \frac{S_{big}}{S_{little}} \tag{3}$$

$$t = \frac{|\overline{X} - \mu|}{s}\sqrt{n} \tag{4}$$

CONCLUSIONS

To summarize, a dual-quenching ECL biosensor based on a ECL−RET novel pair ($GdPO_4$:Eu as the donor and Pd@Cu_2O as the acceptor) was constructed with the low excited potential to maintain protein bioactivity. First, the novel ECL self-enhanced emitter $GdPO_4$:Eu was prepared, and the oxidation−reduction pair Eu^{3+}/Eu^{2+} would be produced under voltage excitation to gain stronger ECL intensity than $GdPO_4$ itself. Furthermore, Pd@Cu_2O was applied to act as a quenching probe based on the satisfied overlaps between its UV−vis with ECL intensity of $GdPO_4$:Eu. CD was utilized to prove the fact of irreversible damage to proteins at excessive positive potentials, and fortunately, the satisfactory ECL intensity of the novel emitter $GdPO_4$:Eu in the potential range from −1.15 to 0 V (vs Ag/AgCl) solved this problem well. Compared with some previous research works, the novel luminophor in this work has the advantages of large specific surface area, strong electrode fixation, and high luminescence with low potential at the same time. Even more surprising is that the proposed system obtained a super low even unprecedented detection limit of 0.402 fg/mL (S/N = 3), which indicated that the PCT ultrasensitive analysis can be achieved without serum sample purification. The established system with a good sensitivity would first not only investigate the ECL behavior of $GdPO_4$:Eu but also develop potential in the related disease diagnosis and clinical analysis in the years to come.

ASSOCIATED CONTENT

Supporting Information

The Supporting Information is available free of charge on the ACS Publications website at DOI: 10.1021/acssensors.9b01552.

Materials and reagents, synthesis of the APF resin template, synthesis of the APF@$Gd(OH)CO_3$ precursor, optimization of the experimental conditions, reproducibility, stability, and specificity of the immunosensor, characterization of materials by SEM, TEM images, and TEM mapping, ECL intensity of $GdPO_4$ and $GdPO_4$:Eu, mechanism investigation of the "Signal on−off" system, simulation parameters of the equivalent circuit components, developed ECL biosensors for detecting PCT compared to other published ECL biosensors, and recoveries of PCT in serum samples (PDF)

AUTHOR INFORMATION

Corresponding Author

*E-mail: Mahongmin2002@126.com.

ORCID

Hongmin Ma: 0000-0002-7061-8944

Qin Wei: 0000-0002-3034-8046

Huangxian Ju: 0000-0002-6741-5302

Notes

The authors declare no competing financial interest.

ACKNOWLEDGMENTS

This study was supported by the National Key Scientific Instrument and Equipment Development Project of China (no. 21627809), National Natural Science Foundation of China (nos. 21675063, 21575050, 21777056, 21505051, 21427808), and Jinan Scientific Research Leader Workshop Project (2018GXRC024).

REFERENCES

(1) Xue, J.; Yang, L.; Wang, H.; Yan, T.; Fan, D.; Feng, R.; Du, B.; Wei, Q.; Ju, H. Quench-type Electrochemiluminescence Immunosensor for Detection of Amyloid Beta-protein Based on Resonance Energy Transfer from Luminol@SnS_2-Pd to Cu Doped WO_3 Nanoparticles. *Biosens. Bioelectron.* **2019**, *133*, 192−198.

(2) Cao, J.-T.; Wang, Y.-L.; Zhang, J.-J.; Dong, Y.-X.; Liu, F.-R.; Ren, S.-W.; Liu, Y.-M. Immuno-Electrochemiluminescent Imaging of Single Cell Based on Functional Nanoprobes of Heterogeneous $Ru(bpy)_3^{2+}$@SiO_2/Au Nanoparticles. *Anal. Chem.* **2018**, *90*, 10334−10339.

(3) Cao, J.-T.; Yang, J.-J.; Zhao, L.-Z.; Wang, Y.-L.; Wang, H.; Liu, Y.-M.; Ma, S.-H. Graphene Oxide@gold Nanorods-based Multiple-assisted Electrochemiluminescence Signal Amplification Strategy for Sensitive Detection of Prostate Specific Antigen. *Biosens. Bioelectron.* **2018**, *99*, 92−98.

(4) Du, F.-K.; Zhang, H.; Tan, X.-C.; Yan, J.; Liu, M.; Chen, X.; Wu, Y.-Y.; Feng, D.-F.; Chen, Q.-Y.; Cen, J.-M.; Liu, S.-G.; Qiu, Y.-Q.; Han, H.-Y. $Ru(bpy)_3^{2+}$-Silica@Poly-L-lysine-Au as Labels for Electrochemiluminescence Lysozyme Aptasensor Based on 3D Graphene. *Biosens. Bioelectron.* **2018**, *106*, 50−56.

(5) Du, J.; Liu, M.; Lou, X.; Zhao, T.; Wang, Z.; Xue, Y.; Zhao, J.; Xu, Y. Highly Sensitive and Selective Chip-based Fluorescent Sensor for Mercuric Ion: Development and Comparison of Turn-on and Turn-off Systems. *Anal. Chem.* **2012**, *84*, 8060−8066.

(6) Bruce, D.; Richer, M. M. Green Electrochemiluminescence from Ortho-Metalated Tris(2-phenylpyridine)iridium(III). *Anal. Chem.* **2002**, *74*, 1340−1342.

(7) (a) Dostalova, S.; Cerna, T.; Hynek, D.; Koudelkova, Z.; Vaculovic, T.; Kopel, P.; Hrabeta, J.; Heger, Z.; Vaculovicova, M.; Eckschlager, T.; Stiborova, M.; Adam, V. Site-Directed Conjugation of Antibodies to Apoferritin Nanocarrier for Targeted Drug Delivery to Prostate Cancer Cells. *ACS Appl. Mater. Interfaces* **2016**, *8*, 14430−14441. (b) Du, J.; Wang, H.; Yang, M.; Zhang, F.; Wu, H.; Cheng, X.; Yuan, S.; Zhang, B.; Li, K.; Wang, Y.; Lee, H. Highly Efficient Hydrogen Evolution Catalysis Based on MoS_2 /CdS/TiO_2 Porous Composites. *Int. J. Hydrogen Energy* **2018**, *43*, 9307−9315.

(8) Jia, Y.; Yang, L.; Xue, J.; Zhang, N.; Fan, D.; Ma, H.; Ren, X.; Hu, L.; Wei, Q. Bioactivity-Protected Electrochemiluminescence Biosensor Using Gold Nanoclusters as the Low-Potential Luminophor and Cu_2S Snowflake as Co-reaction Accelerator for Procalcitonin Analysis. *ACS Sens.* **2019**, *4*, 1909−1916.

DOI: 10.1021/acssensors.9b01552
ACS Sens. 2019, 4, 2825−2831

(9) Feng, Q.-M.; Shen, Y.-Z.; Li, M.-X.; Zhang, Z.-L.; Zhao, W.; Xu, J.-J.; Chen, H.-Y. Dual-Wavelength Electrochemiluminescence Ratiometry Based on Resonance Energy Transfer between Au Nanoparticles Functionalized g-C_3N_4 Nanosheet and $Ru(bpy)_3^{2+}$ for MicroRNA Detection. *Anal. Chem.* **2016**, *88*, 937−944.
(10) Xue, H.; Zhao, J.; Zhou, Q.; Pan, D.; Zhang, Y.; Zhang, Y.; Shen, Y. Boosting the Sensitivity of a Photoelectrochemical Immunoassay by Using SiO_2@polydopamine Core−Shell Nanoparticles as a Highly Efficient Quencher. *ACS Appl. Nano. Mater.* **2019**, *2*, 1579−1588.
(11) Yoon, Y.-s.; Lee, B.-I.; Lee, K. S.; Heo, H.; Lee, J. H.; Byeon, S.-H.; Lee, I. S. Fabrication of A Silica Sphere with Fluorescent and MR Contrasting $GdPO_4$ Nanoparticles from Layered Gadolinium Hydroxide. *Chem. Commun.* **2010**, *46*, 3654−3656.
(12) Zhang, L.; Jiu, H.; Fu, Y.; Sun, Y.; Chen, P.; Li, Y.; Ma, S. Facile Synthesis and Luminescence of $GdPO_4$:Eu Hollow Microspheres by A Sacrificial Template Route. *Mater. Lett.* **2013**, *101*, 47−50.
(13) Halappa, P.; Mathur, A.; Marie-Helene, D.; Shivakumara, C. Alkali Metal Ion Co-doped Eu^{3+} Activated $GdPO_4$ Phosphors: Structure and Photoluminescence Properties. *J. Alloys Compd.* **2018**, *740*, 1086−1098.
(14) Xu, Z.; Cao, Y.; Li, C.; Ma, P. A.; Zhai, X.; Huang, S.; Kang, X.; Shang, M.; Yang, D.; Dai, Y.; Lin, J. Urchin-like $GdPO_4$ and $GdPO_4$:Eu^{3+} Hollow Spheres − hydrothermal Synthesis, Luminescence and Drug-delivery Properties. *J. Mater. Chem.* **2011**, *21*, 3686−3693.
(15) Wu, H.; Yang, X.; Yu, X.; Jie, L.; Hong, Y.; Lv, H.; Yin, K. Preparation and Optical Properties of Eu^{3+}/Eu^{2+} in Phosphors Based on Exchanging Eu^{3+}-zeolite 13X. *J. Alloys Compd.* **2009**, *480*, 867−869.
(16) Zeng, W.-J.; Liao, N.; Lei, Y.-M.; Zhao, J.; Chai, Y.-Q.; Yuan, R.; Zhuo, Y. Hemin as Electrochemically Regenerable Co-reaction Accelerator for Construction of An Ultrasensitive PTCA-based Electrochemiluminescent Aptasensor. *Biosens. Bioelectron.* **2018**, *100*, 490−496.
(17) Hara, M.; Kondo, T.; Komoda, M.; Ikeda, S.; Kondo, J. N.; Domen, K.; Hara, M.; Shinohara, K.; Tanaka, A. Cu_2O as a Photocatalyst for Overall Water Splitting under Visible Light Irradiation. *Chem. Commun.* **1998**, 357−358.
(18) Lin, J.; Hao, W.; Shang, Y.; Wang, X.; Qiu, D.; Ma, G.; Chen, C.; Li, S.; Guo, L. Direct Experimental Observation of Facet-Dependent SERS of Cu_2O Polyhedra. *Small* **2018**, *14*, 1703274.
(19) Kolmakov, A.; Klenov, D. O.; Lilach, Y.; Stemmer, S.; Moskovits, M. Enhanced Gas Sensing by Individual SnO_2 Nanowires and Nanobelts Functionalized with Pd Catalyst Particles. *Nano Lett.* **2005**, *5*, 667−673.
(20) Rej, S.; Wang, H.-J.; Huang, M.-X.; Hsu, S.-C.; Tan, C.-S.; Lin, F.-C.; Huang, J.-S.; Huang, M. H. Facet-dependent Optical Properties of Pd-Cu_2O Core-shell Nanocubes and Octahedra. *Nanoscale* **2015**, *7*, 11135−11141.
(21) Zhao, G.; Wang, Y.; Li, X.; Yue, Q.; Dong, X.; Du, B.; Cao, W.; Wei, Q. Dual-Quenching Electrochemiluminescence Strategy Based on Three-Dimensional Metal-Organic Frameworks for Ultrasensitive Detection of Amyloid-*β*. *Anal. Chem.* **2019**, *91*, 1989−1996.
(22) Wang, C.; Zhang, N.; Wei, D.; Feng, R.; Fan, D.; Hu, L.; Wei, Q.; Ju, H. Double Eectrochemiluminescence Quenching Effects of Fe_3O_4@PDA-Cu_XO towards Self-enhanced $Ru(bpy)_3^{2+}$ Functionalized MOFs with Hollow Structure and It Application to Procalcitonin Immunosensing. *Biosens. Bioelectron.* **2019**, *142*, 111521.
(23) Wu, D.; Wang, Y.; Li, Y.; Wei, Q.; Hu, L.; Yan, T.; Feng, R.; Yan, L.; Du, B. Phosphorylated Chitosan/$CoFe_2O_4$ Composite for the Efficient Removal of Pb(II) and Cd(II) from Aqueous Solution: Adsorption Performance and Mechanism Studies. *J. Mol. Liq.* **2019**, *277*, 181−188.
(24) Zhao, J.; Niu, W.; Zhang, L.; Cai, H.; Han, M.; Yuan, Y.; Majeed, S.; Anjum, S.; Xu, G. A Template-Free and Surfactant-Free Method for High-Yield Synthesis of Highly Monodisperse 3-Aminophenol−Formaldehyde Resin and Carbon Nano/Microspheres. *Macromolecules* **2013**, *46*, 140−145.
(25) Jia, Y.; Yang, L.; Feng, R.; Ma, H.; Fan, D.; Yan, T.; Feng, R.; Du, B.; Wei, Q. MnCO3 as a New Electrochemiluminescence Emitter for Ultrasensitive Bioanalysis of *β*-Amyloid1-42 Oligomers Based on Site-Directed Immobilization of Antibody. *ACS Appl. Mater. Interfaces* **2019**, *11*, 7157−7163.
(26) Salehnia, F.; Hosseini, M.; Ganjali, M. R. Enhanced Electrochemiluminescence of Luminol by An in Situ Silver Nanoparticle-decorated Graphene Dot for Glucose Analysis. *Anal. Methods* **2018**, *10*, 508−514.
(27) Nie, Y.; Zhang, P.; Wang, H.; Zhuo, Y.; Chai, Y.; Yuan, R. Ultrasensitive Electrochemiluminescence Biosensing Platform for Detection of Multiple Types of Biomarkers toward Identical Cancer on a Single Interface. *Anal. Chem.* **2017**, *89*, 12821−12827.
(28) Chen, X.; Liu, Y.; Ma, Q. Recent Advances in Quantum Dot-based Electrochemiluminescence Sensors. *J. Mater. Chem. C* **2018**, *6*, 942−959.
(29) Yu, Y.-Q.; Zhang, H.-Y.; Chai, Y.-Q.; Yuan, R.; Zhuo, Y. A Sensitive Electrochemiluminescent Aptasensor Based on Perylene Derivatives as A Novel Co-reaction Accelerator for Signal Amplification. *Biosens. Bioelectron.* **2016**, *85*, 8−15.
(30) Zou, G.; Ju, H. Electrogenerated Chemiluminescence from A CdSe Nanocrystal Film and Its Sensing Application in Aqueous Solution. *Anal. Chem.* **2004**, *76*, 6871−6876.
(31) Amouzegar, K.; Savadogo, O. Electrocatalytic Hydrogenation of Phenol on Dispersed Pt: Effect of Metal Electrochemically Active Surface Area and Electrode Material. *J. Appl. Electrochem.* **1997**, *27*, 539−542.
(32) Yang, Z.; Shao, X.; Han, Y.; Zhang, H. Detection of Procalcitonin (PCT) Using the Double Antibody Sandwich Method Based on Fluorescence Resonant Energy Transfer Between Upconversion Nanoparticles and Quantum Dots. *Anal. Methods* **2018**, *10*, 1015−1022.
(33) Xue, J.; Yang, L.; Jia, Y.; Zhang, Y.; Wu, D.; Ma, H.; Hu, L.; Wei, Q.; Ju, H. Dual-quenching electrochemiluminescence resonance energy transfer system from Ru-In2S3 to *α*-MoO3-Au based on protect of protein bioactivity for procalcitonin detection. *Biosens. Bioelectron.* **2019**, *142*, 111524.
(34) Dobie, R. A.; Wilson, M. J. A Comparison of t Test, F Test, and Coherence Methods of Detecting Steady-state Auditory-evoked Potentials, Distortion-product Otoacoustic Emissions, or Other Sinusoids. *J. Acoust. Soc. Am.* **1996**, *100*, 2236−2246.

DOI: 10.1021/acssensors.9b01552
ACS Sens. 2019, 4, 2825−2831